Flexible and Printed Electronics

ACCEPTED MANUSCRIPT

Direct writing of stretchable metal flake conductors: improved stretchability and conductivity by combining differently sintered materials

To cite this article before publication: Md Saifur Rahman *et al* 2020 *Flex. Print. Electron.* in press https://doi.org/10.1088/2058-8585/ab8f22

Manuscript version: Accepted Manuscript

Accepted Manuscript is “the version of the article accepted for publication including all changes made as a result of the peer review process, and which may also include the addition to the article by IOP Publishing of a header, an article ID, a cover sheet and/or an ‘Accepted Manuscript’ watermark, but excluding any other editing, typesetting or other changes made by IOP Publishing and/or its licensors”

This Accepted Manuscript is **© 2020 IOP Publishing Ltd**.

During the embargo period (the 12 month period from the publication of the Version of Record of this article), the Accepted Manuscript is fully protected by copyright and cannot be reused or reposted elsewhere.
As the Version of Record of this article is going to be / has been published on a subscription basis, this Accepted Manuscript is available for reuse under a CC BY-NC-ND 3.0 licence after the 12 month embargo period.

After the embargo period, everyone is permitted to use copy and redistribute this article for non-commercial purposes only, provided that they adhere to all the terms of the licence https://creativecommons.org/licences/by-nc-nd/3.0

Although reasonable endeavours have been taken to obtain all necessary permissions from third parties to include their copyrighted content within this article, their full citation and copyright line may not be present in this Accepted Manuscript version. Before using any content from this article, please refer to the Version of Record on IOPscience once published for full citation and copyright details, as permissions will likely be required. All third party content is fully copyright protected, unless specifically stated otherwise in the figure caption in the Version of Record.

View the article online for updates and enhancements.

This content was downloaded from IP address 130.63.39.119 on 22/05/2020 at 03:43

IOP Publishing Flexible and Printed Electronics

Direct Writing of Stretchable Metal Flake Conductors: Improved Stretchability and Conductivity by Combining Differently Sintered Materials

Md Saifur Rahman and Gerd Grau

Department of Electrical Engineering and Computer Science, York University, Toronto, Canada

Email: grau@eecs.yorku.ca

Abstract

Stretchable and flexible electronics with elastic interconnects is critical for electronics to be compatible with wearable applications. Especially fabricating such interconnects with printing technology promises rapid, low-cost, and mass manufacturing. Here, a novel direct-write manufacturing process is presented for a stretchable conductor using an extrusion printer and a micron size silver flake ink as the conductive material without expensive nanomaterials. Conductivity increases as the sintering temperature is increased but at the cost of limited stretchability. To overcome this trade-off, we place one mildly sintered line on top of a fully sintered line to create a hybrid serpentine feature. These two lines of a hybrid feature have two different stretchability-conductivity profiles, synergistically improving both the stretchability and conductivity. With this method, a maximum stretchability of 120% strain is obtained with a minimal change in resistance by a factor of 2.8. This stretchable conductor can endure more than 250 cycles of stretching and releasing under 40% strain. The aggregate electrical conductivity is in the range of $4.74*10^4$ S/cm, which is far superior to any carbon filler based printable composites.

Keywords: Stretchable electronics, stretchable conductors, wearable electronics, printed electronics, direct-write, extrusion printing, silver flake ink

1 Introduction

In a world where conventional rigid electronics are ubiquitous, a need for deformable and flexible electronics is growing. Highly conductive yet naturally stretchable conductors are a crucial enabler for flexible and stretchable electronics. The domain of flexible conductors has seen remarkable advancements due to the increasing need for real-time health care monitoring [1], wearable displays [2], organic solar cells [3], tactile sensors [4], stretchable optoelectronics [5] and smart textiles [6]. In particular, the interest in using traditional printing techniques for manufacturing of such conductors is growing due to the added benefits of scalability and low-cost fabrication.

Accepted Manuscript

© 2020 IOP Publishing Ltd

The goal is to introduce flexibility (ability to bend and twist to have conformation with curvilinear surfaces) and the capability of maintaining a conductive network under large strains as well as the ability to restore properties after releasing strain [7]. One common approach is to fabricate a stretchable conductor with conventional conductive materials with special structural designs or topographical features to dissipate the strain. Representative examples include out of plane buckling [8], serpentine-shaped [9], kirigami-patterned [10] or micro-cracked topography [11] with conductive features of gold [10], aluminum [12], and indium tin oxide [13] on stretchable elastomeric substrates. Unfortunately, these strategies always ultimately suffer from cracks owing to the rigidity of the abovementioned conventional materials [14][15]. Moreover, they often don't use rapid low-cost manufacturing processes such as printing [16] with the metal deposition requiring cleanroom lithography and sputtering. Another approach uses microfluidics, replacing wires with filled microchannels of liquid metals [17]. This is promising but needs costly liquid metal such as Gallium-Indium or Gallium-Indium-Tin. Besides, it requires several steps of soft lithography to create these micro-channels, which renders this method difficult to employ in large-area integration [15]. Forming internal periodic and deformable pores [18,19] can be an alternative to minimize the stress applied to the materials. Mainly vacuum deposition processes are used, and the material cannot be used as a printable fluid. Another extensively researched solution are conductive nanocomposites comprising of conductive fillers in an elastomeric matrix. The polymeric matrix maintains the elasticity while acquiring the electrical properties of the embedded filler. Various fillers have been studied such as carbon derived materials including carbon nanotubes (CNT) [20], graphene flakes [21], conducting polymers [22] as well as metallic nanowires [23], nanosheets [24], and nanoparticles [25]. Whichever conductive fillers are used, a percolation network is always created. A downside of such nanomaterials is generally the high cost.

For fabrication of stretchable electrodes, printing-based methods have attracted significant attention due to the advantages of inherent compatibility with flexible substrates, low cost, rapid prototyping, and manufacturing scalability. The printing of stretchable interconnects is still in the development stage with several research groups putting efforts into this area. Tabatabai et al. demonstrated microcontact printing of liquid metal, e.g., Gallium-Indium alloy on an Ecoflex substrate [26]. The printhead carrying the functional ink is in direct contact with the substrate. The variation of resistance of such material while stretching is fairly low, $\Delta R/R0=170\%$ with 100% stretching [27]. However, the contact printing of such material is a very time-consuming process; each time the printhead needs to deposit a droplet of Eutectic Gallium-Indium (EGaIn), it goes to a container filled with EGaIn to pick one droplet and then deposit it onto the substrate [28]. Moreover, the natural oxidation of EGaIn makes it challenging to deposit smaller droplets; hence, a low resolution is obtained (linewidth is close to 400 μm). Although challenging, recently extrusion-based printing of EGaIn has also gained attention due to the potential for 2.5D or 3D interconnect printing that enables integration with 3D objects [29–31]. Other than liquid metals, the most common material for printing of stretchable conductors are high aspect ratio filler based/embedded composites with a few exceptions of spherical nanoparticle filler based inks [32,33]. Spherical nanoparticles are a poor filler for stretchable electrodes as contact points are limited to adjacent filler material owing to their spherical shape. Thus, the reported value for the maximum stretching is typically limited to 30%-40% [28]. Inkjet printing, a popular contact-less printing technique is used in numerous ways for fabricating stretchable electrodes with silver nanowires [34,35]. However, to avoid nozzle clogging, often a sonication-induced scission step is performed to decrease the nanowires' length, which, in turn, reduces the efficacy of the NW's network while stretching. As a result, the stretchability of an inkjet-printed silver nanowire electrodes does not surpass 75% strain. Aerosol jet printing, an aerodynamically focused contact-less deposition technique, is also used to fabricate stretchable electrodes with silver nanowires [36]. However, this process requires a costly printing apparatus with a complicated

Accepted Manuscript

© 2020 IOP Publishing Ltd

ink tuning process [28]. Carbon-based ink with high aspect ratio filler such as single-walled carbon nanotubes or graphene is used as a material for contact printing such as screen printing [37] and gravure printing [38]. Material wise, these inks suffer from low conductivity (typically below 100 S/cm) even though they have superior stretchability (sometimes up to 400% of strain). These contact printing methods need a mask or stencil with less flexibility in changing the pattern and added cost. Conversely, extrusion printing, also known as direct writing, is a promising digital printing method for printed electronics. This method combines the advantages of inkjet printing and screen printing. Pressurized ink is delivered through a scanned nozzle to the substrate. It has the ability to change the pattern on the fly with larger flexibility in ink material, be it viscosity (100 - $3x10^5$ mPa.s) or compositional flexibility [39].

Figure 1(a) shows a cross-sectional schematic of a screw-based extrusion printer. The rotary motion of the screw vertically moves the piston, which pressurizes the ink and extrudes ink through the nozzle. The ink's viscosity, solvent drying rate, the nozzle's inner diameter, printing speed, and printing height are the parameters for tuning to achieve an optimal linewidth. Conductive paste, fillers with a high aspect ratio, and an elastomeric matrix are the primary choices of materials. Ahn et al. realized stretchable silver interconnects with an ink based on spherically shaped silver nanoparticles using micro-extrusion enabled omnidirectional printing [40]. It involves a pre-strained spring that supports a straight line printed onto it. As the ink is nonbrittle, the straight line assumes an out-of-plan serpentine shape after the removal of the spring. Though this micro-extrusion can enable very fine features (~2 μm linewidth), the maximum stretchability is at best 25% strain.

Here, we report a stretchable conductor by printing micron-sized metal flake ink to form co-planar serpentine-like features with an extrusion printer and then encasing them between two Polydimethylsiloxane (PDMS) layers. Thermal curing is typically used to improve the conductivity of such materials. However, the stretchability of these traces decreases with thermal curing. To solve this problem, we demonstrate here a hybrid structure, one fully sintered and one partially sintered feature on top of each other, with improved overall stretchability (up to 120% strain) and conductivity ($4.74*10^4$ S/cm) compared with one single trace. Similar synergistic improvement of both the stretchability and conductivity in a hybrid structure has been reported in literature combining two distinct materials with different stretchability-conductivity profiles. Graphene has been combined with metal nanowires [41] and sintered metal nanoparticles have been combined with liquid metal [42]. With our approach, the fabrication method is simple to implement and scalable, the material is relatively low cost, and only a single material is needed. As the fully sintered line develops cracks at relatively low strain, the second less well-sintered line, which is less conductive yet more stretchable, bridges the gap between two segments of the fully sintered trace. We have developed different hybrid features with different sintering temperatures of the second line that resides on top of the sintered line. Stretchability is discussed in detail with the aid of optical micrographs and electron microscopy images of surface morphology. Simple resistive modeling correctly predicts the effect of crack formation on the transition in normalized resistance. Finally, dynamic strain testing, i.e., repeated stretching and releasing cycles up to a fixed uniaxial strain, is evaluated to test the endurance of these stretchable interconnects.

2 Materials and Methods

Serpentine features were printed with a commercial screen-printable silver flake ink (Creative Materials 120-07) with a flake size of 5-20 μm. This ink has a thermoplastic polyurethane matrix with silver flakes as the conductive filler. The viscosity of the ink (26,000-30,000 cps) is in the acceptable range for extrusion printing. A commercial extrusion printer based on screw motion dispensing (Voltera V1) is used for printing serpentine

Accepted Manuscript

© 2020 IOP Publishing Ltd

lines with a nozzle size of 220 μm. Degassed PDMS solution (Sylgard 184, silicone, base to curing agent ratio 10:1) is deposited as a 0.5 mm thick layer on PFOTS (Trichloro(1H,1H,2H,2H-perfluorooctyl)silane) treated hydrophobic glass using blade coating with a glass spacer to define the PDMS thickness. Before the thermal curing of the PDMS, two copper (Cu) foil pieces are placed on opposite sides of the substrate to be used as electrodes during electrical measurements.

We choose serpentine features, a spring-like form, consisting of a 2D oscillation with a repeating unit of a half-circle. The tortuousness of this feature reduces stress within the line segments compared to a straight line when it is subjected to uniaxial strain [43]. The extrusion printer prints the whole serpentine with two contact pads on top of the cured PDMS substrate. These pads are placed in such a way that they are also in contact with the Cu foil electrodes. Figure 1(b) describes the whole process, from fabricating the PDMS layer to printing on top of it.

For comparing the stretchability and conductivity, several samples were prepared with a single serpentine feature sintered at different temperatures, ranging from 30°C to 140°C for 1 hour. After printing, the same blade coating method was used to deposit another PDMS layer (1mm thick) on top of the printed layer. We found that with increasing sintering temperature, the conductivity is increased while the stretchability is decreased. With this information, we fabricated hybrid traces consisting of two parallel layers, one mildly sintered and one fully sintered printed line. For fabricating such traces, the first printed trace remains in the printer and is sintered fully with the built-in hot plate of the printer at 140°C for 60 minutes. Then, the next pattern, which is identical to the bottom pattern, is printed on top of the fully sintered line. Two different temperatures for the thermal curing of the top lines were studied, 40°C and 60°C. The same blade coating method as before was used to encase the printed layer with the second layer of PDMS.

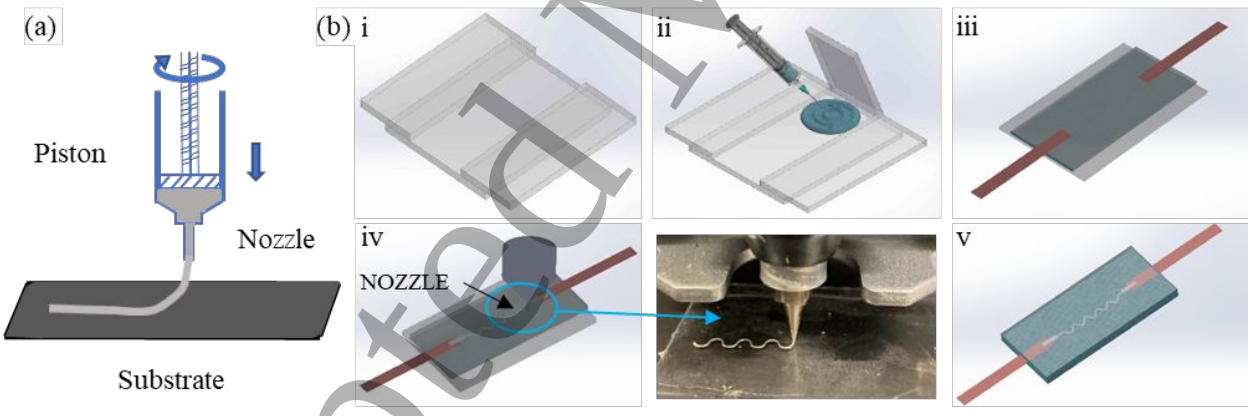


Figure 1. (a) Screw-based extrusion of functional ink: the piston's vertical movement extrudes the ink through the nozzle, the piston is controlled by the screw's rotary motion. (b) Fabrication method for one single line: (i-ii) Blade coating to deposit a 0.5 mm thick PDMS layer on hydrophobic glass. (iii) Two Cu tapes are placed on opposite sides of the cured PDMS layer. (iv) Serpentine lines with contact pads are printed on top of the PDMS. The marked area shows a photograph of the extrusion printer printing through a nozzle with an inner diameter of 220 μm. (v) Encasing with a second PDMS layer is also performed with the same blade coating method before release from the glass.

Accepted Manuscript

© 2020 IOP Publishing Ltd

For tensile testing, dumbbell-shaped specimens were fabricated to improve gripping of the ends of the sample. A 3D printed die, a negative of the preferred shape, is used to cut out dumbbell-shaped specimens after encasing with the second PDMS layer. Finally, the entire stack is released from the glass holder for mechanical testing. Figure 2 (a-c) depicts the process of producing the dumbbell-shaped specimen.

For measuring the electrical resistance of the serpentine lines, a digital multimeter (Keithley, 2100 series) was used. Conductivity was calculated from the height profiles of these lines, which was measured using stylus profilometry (Alpha-Step D-500, KLA-Tencor). The uniaxial strain was measured using a 3D printed mechanical stage combined with a micromanipulator (Figure 2(d)). The dynamic strain cycle was measured with a Dynamic Mechanical Analyzer (TA instrument, DHR3 with DMA Module). The surface morphology of the silver was studied for different sintering conditions using a Field Emission Gun Scanning Electron Microscope (FEG-SEM, Fisher Quanta 3D).

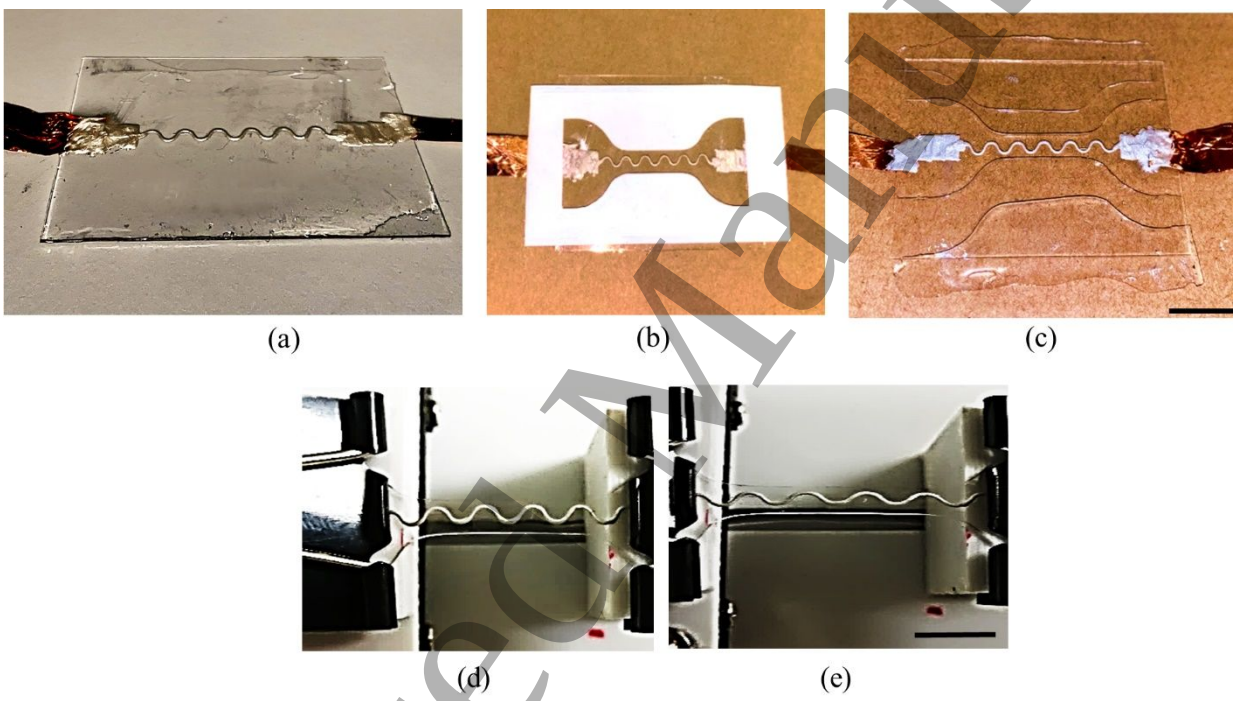


Figure 2. (a) Printed serpentines encased with the second PDMS layer. (b) A 3D printed die is placed on the PDMS to cut out the dumbbell shape. (c) The dumbbell-shaped sample in the middle right after cutting. The scale bar represents 15 mm. Typical printed pattern at (d) 10% strain and (e) 50% strain. The scale bar is equivalent to 10 mm.

3 Results and Discussion

Several serpentine lines were printed and sintered over a range of temperatures, from 30°C to 140°C for 1 hour. There is a decay in stretchability while conductivity increases as the sintering temperature is increased. This is shown in Figure 3(a). From 30°C to 60°C, the conductivity gradually increases from $4.11*10^4$ S/m to $3.02*10^5$ S/m. After that, the conductivity sharply rises to $8.54*10^6$ S/m when the sintering temperature is 85°C. Beyond 85°C, the increase in electrical conductivity is minimal. The maximum conductivity, $9.74*10^6$

Accepted Manuscript

© 2020 IOP Publishing Ltd

S/m is found at 140°C. Conversely, the stretchability, the maximum amount of strain a specimen can endure before electrical resistance becomes infinite, exhibits the opposite trend, declining from 160% to 45%. The sharpest decline also happens at 85°C when the conductivity increases most sharply.

To explain these changes, Scanning Electron Microscopy was performed on both an unsintered line and a line with 90°C sintering for 30 min. Figure 3(b) (i) and (ii) show the surface morphology before and after sintering. From Figure 3(b) (i), one can see that individual flakes are difficult to discern in the unsintered case as they are embedded in the polyurethane matrix. Conversely, Figure 3(b) (ii) shows that after sintering the flakes are more clearly visible without matrix material in between. This indicates that the continuity of the polyurethane matrix has disappeared with 90°C sintering, which exposes the silver flakes to their neighboring flakes. This phenomenon explains the dramatic increase in conductivity and decrease in stretchability at 85°C in Figure 3(a).

Figure 3(c) shows the effect of one strain-relaxation cycle on both 140°C and 40°C sintered serpentine lines. After straining at 40% of the original length, the 140°C sintered line developed cracks at the peak and trough of the serpentines (see Figure 3(c) (i)). Conversely, even with 100% strain, the low temperature sintered serpentine only elongates in these peak and trough regions of the serpentines instead of breaking. To accommodate this elongated line after release of the strain, the material buckles out-of-plane perpendicular to the PDMS layer.

Accepted Manuscript

© 2020 IOP Publishing Ltd

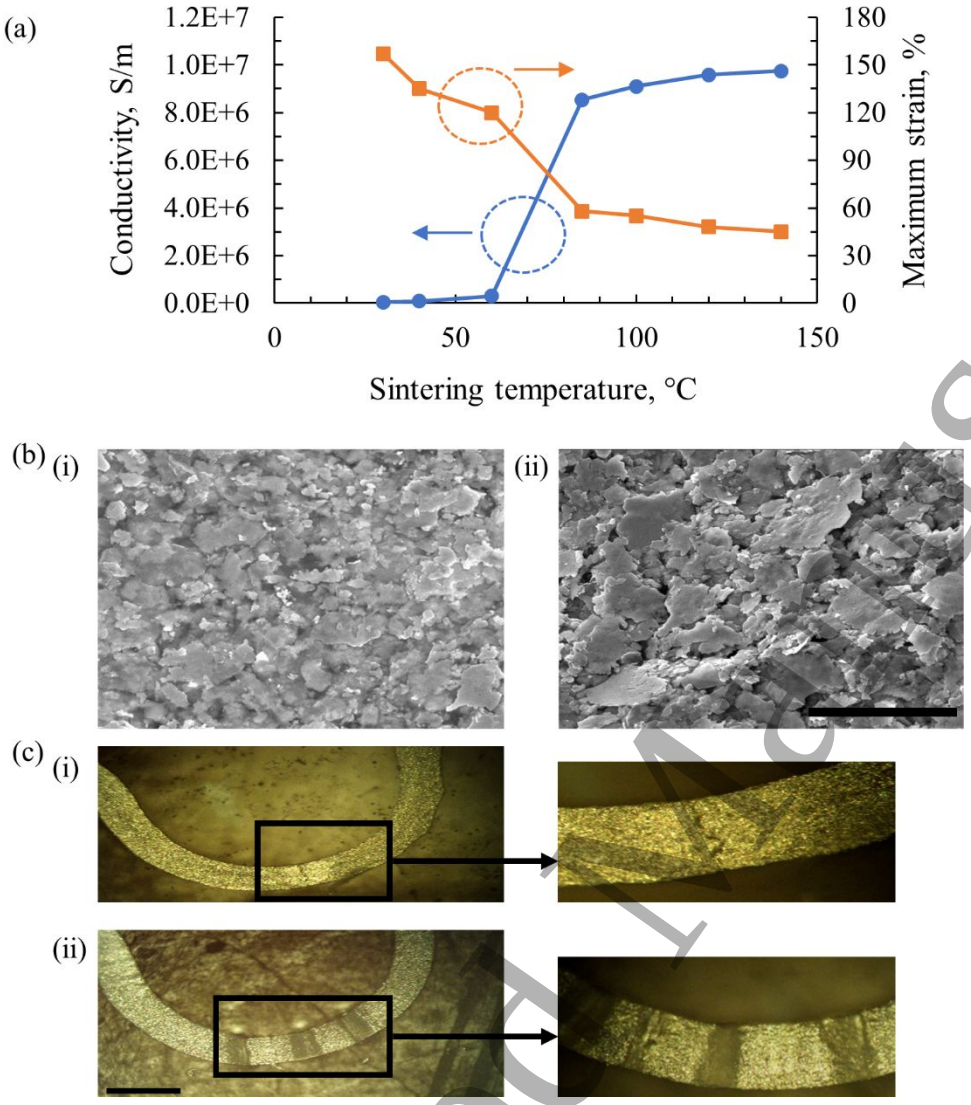


Figure 3. (a) Change of electrical conductivity (blue circles) and maximum strain where resistance becomes infinite (orange squares) as a function of sintering temperature. Lines become more prone to develop cracks with increasing sintering temperature and increasing electrical conductivity. (b) Surface morphology SEM images: (i) 40°C sintered line. A continuous matrix without clear boundaries between individual flakes is found. (ii) 90°C sintered line. Clear flakes without a matrix disrupting current paths can be observed. The scale bar indicates 10 µm. (c) Optical micrographs of silver serpentines after stretching: (i) 140°C sintered line developed crack with only 40% strain, zoomed area shows the nature of the crack (ii) 40°C sintered line stretched without cracks to accommodate 100% strain and developed buckling after release, zoomed area shows the upward deformation of the line due to buckling. The scale bar indicates 500 µm.

In order to overcome the trade-off between conductivity and stretchability, we conceived a hybrid pattern by printing two serpentine lines on top of each other. The two lines are sintered at opposite ends of the temperature range studied here. For example, one line is sintered at 140°C and the other is sintered at 40°C or 60°C. As strain increases, the cracks in the high temperature sintered line will be bridged by the low temperature sintered line, whose conductivity is lower but with higher stretchability than the fully sintered

Accepted Manuscript

© 2020 IOP Publishing Ltd

line. In the lower strain region (0-40% strain), the conductivity will be determined by the fully sintered line, whereas the low temperature sintered line will dominate the stretchability in the higher strain range (40%-120%). Figure 4(a) presents resistance normalized by unstrained resistance R_0 as a function of uniaxial strain for single lines sintered at different temperatures as well as hybrid lines. From this figure, hybrid lines with 40°C sintered top face a sharp transition in normalized resistance when the strain reaches around 45%; however, unlike the fully sintered single line, it is not completely broken and can still conduct current. This transition can be explained by the fact that among the two lines in a hybrid feature, the 140°C sintered line exhibits cracks while the line on top of it, the low temperature sintered line, remains intact. During the electrical resistance measurement, the current follows the unbroken top line which is more resistive but works as a bridge to pass over the cracks. The hybrid line with 60°C sintered top exhibits a much less pronounced transition at 45% strain due to its superior conductivity. In terms of absolute resistance, hybrid lines with both 40°C or 60°C sintered top exhibit resistance close to fully sintered single lines (see Figure 4(b) and Figure S1 for a smaller resistance scale).

Cracks are generated at the peak of each serpentine's half-cycle for a 140°C sintered line (referring to figure 3(c)). Along the line, these cracks keep adding resistance to the total resistance of the hybrid line, owing to the more resistive top line. We modeled the total resistance of a hybrid serpentine line, which explains the resistance increase during the crack formation. Figure 4(c) shows the top and side view of a hybrid line with the modeled resistance for both lines. We know the conductivity of a single line sintered at different temperatures from Figure 3(a). Knowing the crack length, we can calculate the resistance that is added by the bridge of the 40/60°C sintered line. Other than the cracked part, the resistance of the remaining hybrid line R` is calculated by the parallel combination of the two lines (see equation (1)). Here, R_1 and R_2 are the resistance of the 40/60°C sintered line and the sintered line respectively. The length is that of one half-cycle from one crack to the next crack. We measured the crack length, which is the length of the 40/60°C sintered line bridging the crack and responsible for the extra resistance R``. The total resistance for one crack and one-half cycle is calculated by the series combination of R` and R`` (see equation (2)).

$$\frac{1}{R'} = \frac{1}{R_1} + \frac{1}{R_2} \quad (1)$$

$$R = R` + R`` \quad (2)$$

The total resistance of the serpentine is calculated by multiplying the total number of half cycle-crack pairs with R (see the result in Figure 4(d)). For the case of a hybrid feature with a 40°C line, a total of 11 cracks add 0.23 Ω, coming from a total of five full cycles of the serpentine. This amounts to an increase in normalized resistance to about 6 at around 45% strain, where the fully sintered line develops cracks. This calculated resistance jump from modeling compares well with the measured resistance jump, and the modeled and measured resistance follow the same trend with strain, although the model somewhat underestimates the final resistance. The model is more accurate for the 60°C hybrid than the 40°C hybrid, possibly because it does not take into account differences in mechanical properties of the different layers. For the case of a hybrid feature with a 60°C line, these 11 cracks add 0.0238 Ω. This value contributes to the normalized resistance jump to 1.72 at 45% strain, whereas the measured value is 1.71. Hybrid lines with 40°C top at 140% strain and 60°C hybrid lines at 120%. Thus, hybrid lines of fully sintered and partially sintered silver flakes can achieve a stretchable conductor combining low resistance and good stretchability.

There are three strain regimes for such hybrid stretchable conductors: the low strain regime up to the failure point of the fully sintered layer (40%), the medium strain regime up to the failure point of the less sintered layer (120% for 60°C hybrid), and the high strain regime where both layers have failed and conduction is lost.

Accepted Manuscript

© 2020 IOP Publishing Ltd

The best strain regime to operate in depends on the application. For applications that are very sensitive to the resistance of the conductor, for example sensitive measurements, it would be advisable to stay within the low strain regime where resistance only increases by 25% over 40% strain for the 60°C hybrid line. Beyond this strain, resistance undergoes a jump. Such applications likely would not operate in the medium strain regime continuously but may still benefit from the higher ultimate strain offered by the hybrid preventing catastrophic failure in case of short-term large deformations. However, it should be noted that even with this jump the overall resistance is still very low. For example, a line that is 10 cm long in the unstretched state would remain well below 1 Ω even at 120% strain. Therefore, many circuits could be designed such that the resistance of the stretchable conductor is always negligible relative to the resistance of other devices, for example to drive a light-emitting diode (LED).

We considered whether adding a third layer with different sintering conditions would further improve the performance of the hybrid structure. Two different cases were modeled, both with a layer sintered at 140°C and one at 40°C as well as a third layer in between at an intermediate sintering temperature. Performance is only marginally improved as shown in Figure S2. If the third layer is sintered at 100°C, the benefit is very marginal because the 100°C layer is only marginally more stretchable than the 140°C layer (55% vs 45% strain). Having a mid-layer that is almost sintered only contributes by lowering the resistance in the low strain regime. After 55%, the R/R0 value rises to 10 times of the resistance of the unstrained state, which is a bigger relative increase than the two-layer case with 40°C and 140°C because the unstrained resistance is lower with three layers. If the third layer is sintered at 60°C, the benefit would again be marginal. The behavior is very similar to the 60°C-140°C two-layer structure up to the failure point of the 60°C layer (120% strain). Beyond this strain, the 40°C sintered layer dominates, which means resistance increases sharply and ultimate strain is increased to the failure point of the 40°C sintered layer of 140%. One could consider further combinations that might be beneficial for a particular application. An experimental challenge would be that sintering the final layer with 40°C or 60°C could affect the mid-layer, which is also not fully sintered. Further work is needed to study this effect and potentially overcome it with alternative sintering strategies such as photonic annealing.

Accepted Manuscript

© 2020 IOP Publishing Ltd

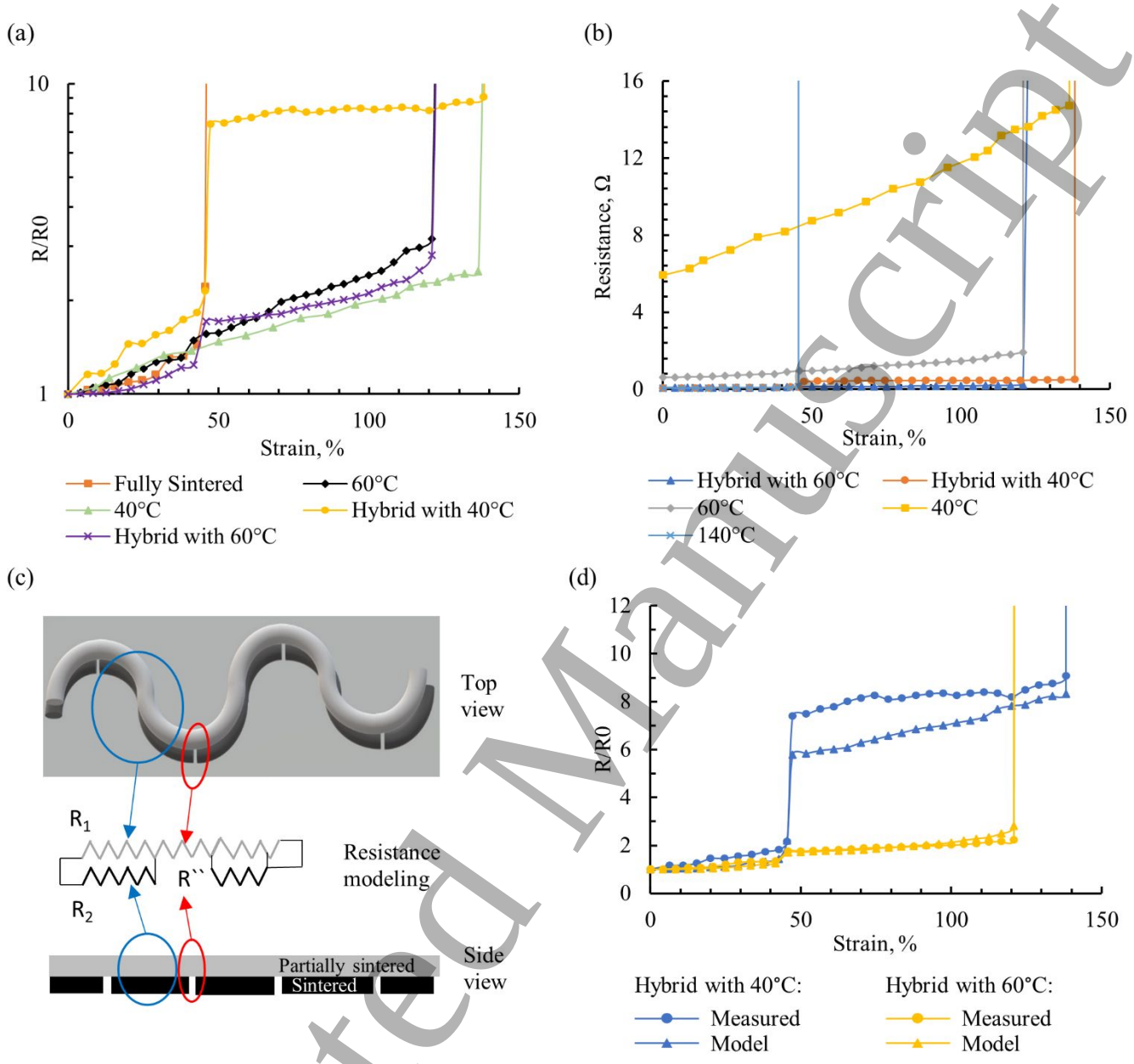


Figure 4. (a) Normalized resistance of single and hybrid lines as a function of strain (log scale to visualize differences for small resistance changes). The hybrid lines, especially with 60°C, can endure a much larger strain range with little change in normalized resistance. (b) The absolute resistance of single and hybrid lines. Although 40°C and 60°C single lines are more stretchable, they have higher resistance. Conversely, hybrid lines exhibit resistance close to fully sintered single lines. (c) Resistance model with top view and side view of hybrid line. The silver line represents the 40°C/60°C sintered top line, the black line represents the fully sintered bottom line. The blue circled region in both top view and side view corresponds to R_1 and R_2 in the resistance modeling, whereas the red circled region represents the crack corresponding to R``. (d) Comparison of the normalized resistance increase predicted by the model and measured experimentally for hybrid lines with 40°C/60°C sintered top line. The 60°C sintered line exhibits better agreement between model and measurement and a lower resistance increase.

Accepted Manuscript

© 2020 IOP Publishing Ltd

Figure 5(a) shows the normalized resistance of the hybrid structure with a 60°C top line for repetitive cycles of 40% strain and a strain rate of 100 μm/s. The resistance gradually increases to about three times of the original resistance over 250 cycles. Notably, the resistance returns to its original level after the release of strain, demonstrating the excellent reversible electromechanical nature of the material. Figure 5(b) shows a small number of cycles of stretching and releasing up to a strain of 40%. The change of R/R0 generally follows the applied strain but also exhibits time-dependent behavior. Initially, R/R0 increases/decreases fast as strain is ramped up/down, which can be attributed to geometrical changes as well as the increasing distance between neighboring silver flakes as strain increases. As the maximum or minimum strain is approached, the change of R/R0 slows down. The resistance peaks before maximum strain is reached, denoted by point 1. This occurs because of stress relaxation of the PDMS film and probably also of the mildly cured thermoplastic ink. This stress relaxation helps the flakes to realign, find new percolation networks, and causes the resistance to decrease from point 1 to 2. Another small peak in resistance can be observed from point 2 to 3 when the strain is released before resistance decreases. Such stress relaxation behavior is common in literature for stretchable conductors on PDMS and both peaks have been observed before, for example in [44,45].

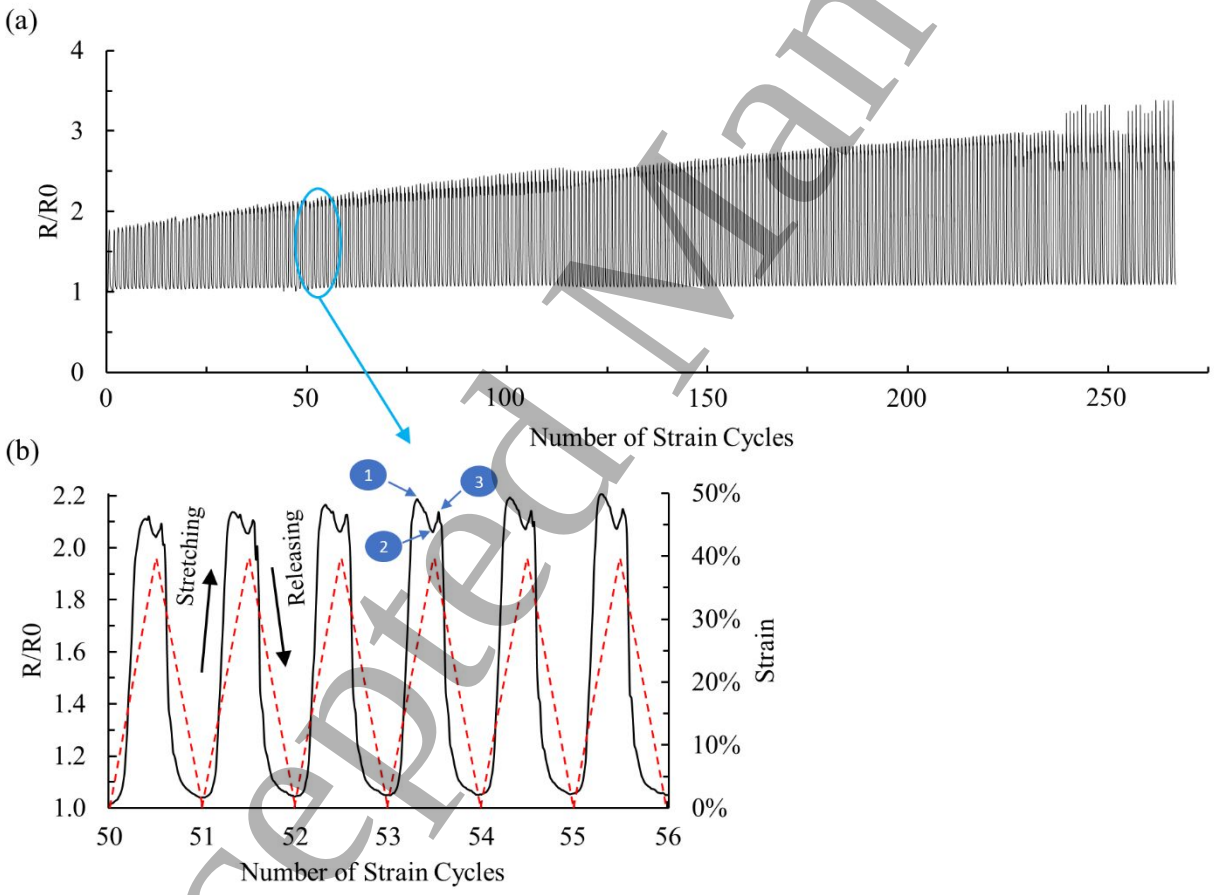


Figure 5. (a) Normalized resistance of a hybrid feature with 60°C top line during repetitive strain and relaxation cycles, with a peak strain value of 40%. The peak resistance in each cycle gradually increases whereas the change in base value is negligible. (b) Normalized resistance for small number of cycles of loading and unloading from 0% to 40% strain. Red dashed line shows applied strain.

Accepted Manuscript

© 2020 IOP Publishing Ltd

4 Conclusions

In summary, a new method is presented to create highly conductive stretchable interconnects with an inexpensive extrusion printer and commercial micron-sized silver flake ink without expensive nanomaterial fillers. There exists a trade-off between conductivity and stretchability for different sintering temperatures of the silver ink. A hybrid serpentine line is demonstrated here by stacking two lines vertically that are sintered at different temperatures. Due to the difference in sintering, one line has more stretchability with less conductivity while the other line has more conductivity and less stretchability. Their different stretchability-conductivity profiles complement each other's properties under strain. While the fully sintered line provides increased overall conductivity, the less sintered line provides more stretchability to the hybrid feature. With this method, hybrid serpentine lines can conduct even at 120% strain with a relative increase in resistance of 2.8 times compared to the unstrained resistance.

Future work using techniques such as thermogravimetric analysis (TGA) combined with X-ray photoelectron spectroscopy (XPS) could be performed on differently sintered material for a mechanistic study of the sintering process of metal flake inks. Especially, how the disruption of the thermoplastic polyurethane matrix creates the percolation network between flakes needs to be studied. More comprehensive modeling of the hybrid lines' resistance change with strain could consider the materials' mechanical properties and could use in-situ measurement of the deformation.

5 Acknowledgements

We acknowledge the support of the Natural Sciences and Engineering Research Council of Canada (NSERC), funding reference number STPGP 521480-18. SEM images were obtained at the Advanced Light and Electron Microscopy Facility at York University.

6 References

[1] Kim Y S, Mahmood M, Lee Y, Kim N K, Kwon S, Herbert R, Kim D, Cho H C and Yeo W H 2019 All-in-One, Wireless, Stretchable Hybrid Electronics for Smart, Connected, and Ambulatory Physiological Monitoring *Advanced Science*

[2] Rogers J A, Bao Z, Baldwin K, Dodabalapur A, Crone B, Raju V R, Kuck V, Katz H, Amundson K, Ewing J and Drzaic P 2001 Paper-like electronic displays: Large-area rubber-stamped plastic sheets of electronics and microencapsulated electrophoretic inks *Proceedings of the National Academy of Sciences of the United States of America* **98** 4835–40

[3] Lipomi D J, Tee B C-K, Vosgueritchian M and Bao Z 2011 Stretchable Organic Solar Cells *Advanced Materials* **23** 1771–5

[4] Zirkl M, Haase A, Fian A, Schön H, Sommer C, Jakopic G, Leising G, Stadlober B, Graz I, Gaar N, Schwödiauer R, Bauer-Gogonea S and Bauer S 2007 Low-Voltage Organic Thin-Film Transistors with

Accepted Manuscript

© 2020 IOP Publishing Ltd

High-k Nanocomposite Gate Dielectrics for Flexible Electronics and Optothermal Sensors *Advanced Materials* **19** 2241–5

[5] Kim J, Salvatore G A, Araki H, Chiarelli A M, Xie Z, Banks A, Sheng X, Liu Y, Lee J W, Jang K I, Heo S Y, Cho K, Luo H, Zimmerman B, Kim J, Yan L, Feng X, Xu S, Fabiani M, Gratton G, Huang Y, Paik U and Rogers J A 2016 Battery-free, stretchable optoelectronic systems for wireless optical characterization of the skin *Science Advances* **2**

[6] Vervust T, Buyle G, Bossuyt F and Vanfleteren J 2012 Integration of stretchable and washable electronic modules for smart textile applications *Journal of the Textile Institute* **103** 1127–38

[7] Kim D-H, Xiao J, Song J, Huang Y and Rogers J A 2010 Stretchable, Curvilinear Electronics Based on Inorganic Materials *Advanced Materials* **22** 2108–24

[8] Xu S, Yan Z, Jang K I, Huang W, Fu H, Kim J, Wei Z, Flavin M, McCracken J, Wang R, Badea A, Liu Y, Xiao D, Zhou G, Lee J, Chung H U, Cheng H, Ren W, Banks A, Li X, Paik U, Nuzzo R G, Huang Y, Zhang Y and Rogers J A 2015 Assembly of micro/nanomaterials into complex, three-dimensional architectures by compressive buckling *Science* **347** 154–9

[9] Choi S, Han S I, Kim D, Hyeon T and Kim D H 2019 High-performance stretchable conductive nanocomposites: Materials, processes, and device applications *Chemical Society Reviews* **48** 1566–95

[10] Wang Z, Zhang L, Duan S, Jiang H, Shen J and Li C 2017 Kirigami-patterned highly stretchable conductors from flexible carbon nanotube-embedded polymer films *Journal of Materials Chemistry C* **5** 8714–22

[11] Filiatrault H L, Carmichael R S, Boutette R A and Carmichael T B 2015 A Self-Assembled, Low-Cost, Microstructured Layer for Extremely Stretchable Gold Films *ACS Applied Materials & Interfaces* **7** 20745–52

[12] Lee J, Yoo B, Lee H, Cha G D, Lee H-S, Cho Y, Kim S Y, Seo H, Lee W, Son D, Kang M, Kim H M, Park Y Il, Hyeon T and Kim D-H 2017 Ultra-Wideband Multi-Dye-Sensitized Upconverting Nanoparticles for Information Security Application *Advanced Materials* **29** 1603169

[13] Song J-K, Son D, Kim J, Yoo Y J, Lee G J, Wang L, Choi M K, Yang J, Lee M, Do K, Koo J H, Lu N, Kim J H, Hyeon T, Song Y M and Kim D-H 2017 Wearable Force Touch Sensor Array Using a Flexible and Transparent Electrode *Advanced Functional Materials* **27** 1605286

[14] Song J, Jiang H, Huang Y and Rogers J A 2009 Mechanics of stretchable inorganic electronic materials *Journal of Vacuum Science & Technology A: Vacuum, Surfaces, and Films* **27** 1107–25

[15] Rogers J A, Someya T and Huang Y 2010 Materials and Mechanics for Stretchable Electronics *Science* **327** 1603–7

[16] Dang W, Vinciguerra V, Lorenzelli L and Dahiya R 2017 Printable stretchable interconnects *Flexible and Printed Electronics* **2**

Accepted Manuscript

© 2020 IOP Publishing Ltd

[17] Noda K, Iwase E, Matsumoto K and Shimoyama I 2010 Stretchable liquid tactile sensor for robot-joints *Proceedings - IEEE International Conference on Robotics and Automation* pp 4212–7

[18] Zhao N, Yang M, Zhao Q, Gao W, Xie T and Bai H 2017 Superstretchable Nacre-Mimetic Graphene/Poly(vinyl alcohol) Composite Film Based on Interfacial Architectural Engineering *ACS Nano* **11** 4777–84

[19] Lee Y-Y, Kang H-Y, Gwon S H, Choi G M, Lim S-M, Sun J-Y and Joo Y-C 2016 A Strain-Insensitive Stretchable Electronic Conductor: PEDOT:PSS/Acrylamide Organogels *Advanced Materials* **28** 1636–43

[20] Sekitani T, Noguchi Y, Hata K, Fukushima T, Aida T and Someya T 2008 A rubberlike stretchable active matrix using elastic conductors *Science*

[21] Jeong Y R, Park H, Jin S W, Hong S Y, Lee S-S and Ha J S 2015 Highly Stretchable and Sensitive Strain Sensors Using Fragmentized Graphene Foam *Advanced Functional Materials* **25** 4228–36

[22] Seol Y G, Trung T Q, Yoon O J, Sohn I Y and Lee N E 2012 Nanocomposites of reduced graphene oxide nanosheets and conducting polymer for stretchable transparent conducting electrodes *Journal of Materials Chemistry* **22** 23759–66

[23] Park J, Choi S, Janardhan A H, Lee S Y, Raut S, Soares J, Shin K, Yang S, Lee C, Kang K W, Cho H R, Kim S J, Seo P, Hyun W, Jung S, Lee H J, Lee N, Choi S H, Sacks M, Lu N, Josephson M E, Hyeon T, Kim D H and Hwang H J 2016 Electromechanical cardioplasty using a wrapped elasto-conductive epicardial mesh *Science Translational Medicine* **8**

[24] Shin M, Song J H, Lim G-H, Lim B, Park J-J and Jeong U 2014 Highly Stretchable Polymer Transistors Consisting Entirely of Stretchable Device Components *Advanced Materials* **26** 3706–11

[25] Park M, Im J, Shin M, Min Y, Park J, Cho H, Park S, Shim M B, Jeon S, Chung D Y, Bae J, Park J, Jeong U and Kim K 2012 Highly stretchable electric circuits from a composite material of silver nanoparticles and elastomeric fibres *Nature Nanotechnology* **7** 803–9

[26] Tabatabai A, Fassler A, Usiak C and Majidi C 2013 Liquid-phase gallium-indium alloy electronics with microcontact printing *Langmuir* **29** 6194–200

[27] Kim H J, Son C and Ziaie B 2008 A multiaxial stretchable interconnect using liquid-alloy-filled elastomeric microchannels *Applied Physics Letters* **92**

[28] Fernandes D F, Majidi C and Tavakoli M 2019 Digitally printed stretchable electronics: A review *Journal of Materials Chemistry C* **7** 14035–68

[29] Yoon Y, Kim S, Kim D, Kauh S K and Lee J 2019 Four Degrees-of-Freedom Direct Writing of Liquid Metal Patterns on Uneven Surfaces *Advanced Materials Technologies* **4** 1800379

Accepted Manuscript

© 2020 IOP Publishing Ltd

[30] Park Y G, An H S, Kim J Y and Park J U 2019 High-resolution, reconfigurable printing of liquid metals with three-dimensional structures *Science Advances* **5** eaaw2844

[31] Cook A, Parekh D P, Ladd C, Kotwal G, Panich L, Durstock M, Dickey M D and Tabor C E 2019 Shear-Driven Direct-Write Printing of Room-Temperature Gallium-Based Liquid Metal Alloys *Advanced Engineering Materials* **21** 1900400

[32] Albrecht A, Bobinger M, Salmerón J F, Becherer M, Cheng G, Lugli P and Rivadeneyra A 2018 Over-stretching tolerant conductors on rubber films by inkjet-printing silver nanoparticles for wearables *Polymers* **10**

[33] Lee J, Chung S, Song H, Kim S and Hong Y 2013 Lateral-crack-free, buckled, inkjet-printed silver electrodes on highly pre-stretched elastomeric substrates *Journal of Physics D: Applied Physics* **46** 105305

[34] Finn D J, Lotya M and Coleman J N 2015 Inkjet printing of silver nanowire networks *ACS Applied Materials and Interfaces* **7** 9254–61

[35] Huang Q, Al-Milaji K N and Zhao H 2018 Inkjet Printing of Silver Nanowires for Stretchable Heaters *ACS Applied Nano Materials* **1** 4528–36

[36] Gandhiraman R P, Jayan V, Han J-W, Chen B, Koehne J E and Meyyappan M 2014 Plasma Jet Printing of Electronic Materials on Flexible and Nonconformal Objects *ACS Applied Materials & Interfaces* **6** 20860–7

[37] Sekitani T, Nakajima H, Maeda H, Fukushima T, Aida T, Hata K and Someya T 2009 Stretchable active-matrix organic light-emitting diode display using printable elastic conductors *Nature Materials* **8** 494–9

[38] Secor E B, Lim S, Zhang H, Frisbie C D, Francis L F and Hersam M C 2014 Gravure Printing of Graphene for Large-area Flexible Electronics *Advanced Materials* **26** 4533–8

[39] Huang Q and Zhu Y 2019 Printing Conductive Nanomaterials for Flexible and Stretchable Electronics: A Review of Materials, Processes, and Applications *Advanced Materials Technologies* **4** 1800546

[40] Ahn B Y, Duoss E B, Motala M J, Guo X, Park S Il, Xiong Y, Yoon J, Nuzzo R G, Rogers J A and Lewis J A 2009 Omnidirectional printing of flexible, stretchable, and spanning silver microelectrodes *Science* **323** 1590–3

[41] Lee M S, Lee K, Kim S Y, Lee H, Park J, Choi K H, Kim H K, Kim D G, Lee D Y, Nam S and Park J U 2013 High-performance, transparent, and stretchable electrodes using graphene-metal nanowire hybrid structures *Nano Letters* **13** 2814–21

[42] Tavakoli M, Malakooti M H, Paisana H, Ohm Y, Green Marques D, Alhais Lopes P, Piedade A P, de Almeida A T and Majidi C 2018 EGaIn-Assisted Room-Temperature Sintering of Silver Nanoparticles for Stretchable, Inkjet-Printed, Thin-Film Electronics *Advanced Materials* **30**

Accepted Manuscript

© 2020 IOP Publishing Ltd

[43] Gray D S, Tien J and Chen C S 2004 High-Conductivity Elastomeric Electronics *Advanced Materials* **16** 393–7

[44] Birchfield D, Jackson X, Pasternak T, Hanson A and Atashbar M 2019 Strain Sensor Fabrication by Means of Laser Carbonization *FLEPS 2019 - IEEE International Conference on Flexible and Printable Sensors and Systems, Proceedings* (Institute of Electrical and Electronics Engineers Inc.)

[45] Chhetry A, Sharifuzzaman M, Yoon H, Sharma S, Xuan X and Park J Y 2019 MoS2-Decorated Laser-Induced Graphene for a Highly Sensitive, Hysteresis-free, and Reliable Piezoresistive Strain Sensor *ACS Applied Materials and Interfaces*

Accepted Manuscript

© 2020 IOP Publishing Ltd